Journal of Basrah Researches (Sciences) **51**(1), 68 (2025)
DOI: https://doi.org/10.56714/bjrs.51.1.6

The Effect of Convolution Theory for Heat Transfer of Unsteady Nanofluid Flow with Presenting an Inclined Magnetic Field

Haedir Abd AlRazak Namoos *, **Abeer Majeed Jasim**

Department of Mathematics, College of Science, University of Basrah, Basrah, Iraq.

ARTICLE INFO

Received 5 January 2025
Revised 7 Febraury 2025
Accepted 15 Febraury 2025
Published 30 June 2025

Keywords:

Q-Homotopy Analysis Method, Laplace Transform, Convolution Theory, Padé Approximate, Variable Thermal Conductivity, Squeezing Unsteady, An Inclination Angle Of An Applied Magnetic Field.

Citation: H. A. A. Namoos , A. M. Jasim, J. Basrah Res. (Sci.) **51**(1), 68 (2025).
DOI:https://doi.org/10.56714/bjrs.51.1.6

ABSTRACT

The study examines unsteady nanofluid heat transfer in a squeezing flow between two parallel plates, using water as the base of fluid with gold (Au), and magnetite (Fe_3O_4) nanoparticles. A new analytical approach (LCP-q-HAM) combining the q-homotopy analysis method, Laplace transform, convolution theory, and Padé approximation is employed to solve nonlinear differential equations that have to do with magnetic field effects and thermal conductivity. Analytical and numerical solutions (using BVP4C) are compared through tables and graphs, analyzing temperature and velocity distributions for various parameters such as nanoparticle volume fraction, Hartmann number, squeeze number, magnetic field angle, and conductivity. The results confirm the effectiveness of the analytical method.

1. Introduction

Heat transfer squeezing unsteady viscous flow between moving plates has gained considerable interest from scientists due to its wide range in many physical applications, including lubrication systems, polymer processing, food processing, hydrodynamical machines, compression, and crop damage from freezing, formation, and dispersion, among other things. Studying the various characteristics of the nanofluids in various geometries has garnered a lot of attention lately. Fluids with additional nanoscale particles are referred to as nanofluids. Water, ethylene glycol, and kerosene oil are examples of common heat transfer fluids that are poor heat conductors. That is, the development of energy-saving heat transfer equipment for power supply depends largely on these heating and cooling fluids. These fluids are mixed with conductive metal nanoparticles to improve and regulate thermal conductivity. Nanofluids are used in fuel cells, medicinal procedures, microelectronics, and other fields. Many researchers interested in the problem of nanofluid flow fields have done a lot of research in this field, as Sreenivasa Somireddy Reddy et al. [1] investigate

*Corresponding author email : haedirnamoos@gmail.com

N: 1817-2695 (Print); 2411-524X (Online)
ine at: https://jou.jobrs.edu.iq

the effects of an inclined magnetic field on heat and mass transfer in turbulent squeeze flow of a viscoelastic fluid.

With an upper-convicted Maxwell model. Abdullah Dawaret et al. [2] the considered problem is solved by two analytical methods called IRPSM, and the homotopy perturbation method (HPM) for a squeezing flow between two parallel plates. Domairry and Hatami [3] looked at the flow analysis between two parallel plates of Cu-water squeezing nanofluid. The problem of very efficient, intelligent techniques have been used to solve the fourth-order nonlinear ordinary differential equations arising from squeezing unsteady nanofluid flow by Ahcene Nouar et al. [4]. Khan et al. [5] studied the squeezing flow of Cu-water or Cu-kerosene nanofluid between two parallel plates while accounting for velocity slip and viscous dissipation. Study approximate analytical unsteady flow and heat transfer analysis of CNTs nanofluid over stretching sheet for the improvement of heat assignment ratio by Ali Rehman et al. [6]. Additionally, Hassan et al. [7] the problem of physical flow on a compressed fluid is solved in Parallel plates through a porous Darcy channel when the fluid moves as a result of the compression of the upper plate towards the expanding lower plate. The problem of compressing fluid flow has been the subject of certain basic research [8–11], where findings show that the heat transfer rate reduces with an excess in the squeezing parameter, it increases with an excess in the nanoparticle volume fraction. The presence of the magnetic field in the imposed problems is important and has received much attention from researchers, such as Eid [12] who looked at the MHD mixed convection of nanofluid flow across an exponentially extending sheet when chemical reactions and heat generation-absorption effects filled up a porous medium. The effects of a magnetic field and heat generation absorption on the passage of a non-Newtonian nanofluid across a permeable stretched surface with suction- injection were investigated by Eid and Mahny [13]. Khaled Al-Farhan et al. [14] Numerical study of natural convective heat transfer of partially heated tall rectangular cavity filled with (Al_2O_3-water) nanofluid. Focuses Yahaya Shagaiya Daniel et al. [15] on the effects of suction as well as thermal radiation, chemical reaction, viscous dissipation, and Joule heating on a two-dimensional natural convective flow of unsteady electrical magnetohydrodynamics (MHD) nanofluid over a linearly permeable stretching sheet. This improvement involves combining the proposed method (q-HAM) with the Laplace transform supported by convolution theory and the Padé approximation [16- 18]. The effect was studied physical parameters on the velocity and temperature distributions for heat transfer of unsteady two-dimensional squeezing flow of a Casson fluid between parallel circular plates is studied [19]. The table below describes all the symbols used in this study.

Nomenclature

$\tilde{p}$	fluid pressure	B_0	electromagnetic induction
$C_{p_{nf}}$	specific heat of nanofluids	φ	angle of inclination magnetic field
$\hat{\rho}_{nf}$	density of nanofluids	Ha	Hartman number
$\check{\mu}_{nf}$	dynamic viscosity of nanofluids	E_c	Eckert number
v_{nf}	kinematic viscosity of nanofluids	P_r	Prandtl number
σ_{nf}	electrical conductivity of nanofluids	w	Nanoparticle volume fraction
$k_{nf}(T)$	variable thermal conductivity	S	squeeze number
σ_f	base fluid	ε	thermal conductivity

The principal interest and aim here is to investigate the effects of an inclined magnetic field, variable thermal conductivity, squeeze number, angle of inclination, and viscous dissipation on the velocity and temperature distributions for time-dependent heat transfer nanofluid flow between two parallel plates. Additionally, the effects of different kinds of nanoparticles such as Au, and Fe_3O_4 are also studied. The governing equations resulting from transformations are resolved using the q-homotopy analysis approach and BVP4C. This means the proposed problem was first analytically solved and then numerically solved. Generally, the main of the present work is to improve the solutions of the q-HAM by combining the proposed method with the Laplace transform supported by convolution theory and the Padé approximation. Features of various flow parameters on Nusselt number and skin friction are discussed. Finally, solution results for LTCP-q-HAM are represented

in several tables and graphs and compared with BVP4C. The thermophysical properties of different nanoparticles are shown in Table (1) as follows:

Table 1. Thermophysical properties of pure water and nanoparticles.

Material	$\rho(kg/m^3)$	$C_\rho(j/kgk)$	$k(W/mk)$	$\sigma(Sm^{-1})$
Clearwater	997.1	4179	0.613	0.05
Au	19300	129	318	4.52×10^7
Fe_3O_4	5180	670	9.7	0.74×10^6

2. Mathematical Formulation:

An unsteady two-dimensional heat transfer of a squeezing flow nanofluid between two infinitely extended parallel plates is under consideration with the effect of slip velocity. This formulation modeling applied a variable strength transverse magnetic field perpendicular to both plates. The definition of distance between two plates $h(t) = \pm l(1-\varphi t)^{1/2}$, where l is the starting point ($t = 0$).

This system has several physical properties, including incompressible flow, no chemical reaction, and viscous dissipation effects are maintained. Figure (1) explains the geometric model of the imposed problems. The following are the governing equations that depict the flow:

$$\frac{\partial u}{\partial x}+\frac{\partial v}{\partial y}=0, \tag{1}$$

$$\left(\frac{\partial u}{\partial t}+u\frac{\partial u}{\partial x}+v\frac{\partial u}{\partial y}\right)=-\frac{1}{\hat{\rho}_{nf}}\frac{\partial \tilde{p}}{\partial x}+\frac{\breve{\mu}_{nf}}{\hat{\rho}_{nf}}\left(\frac{\partial^2 u}{\partial x^2}+\frac{\partial^2 u}{\partial y^2}\right)-\frac{\sigma_{nf}}{\hat{\rho}_{nf}}B_0^2 sin^2\varphi u, \tag{2}$$

$$\frac{\partial T}{\partial t}+u\frac{\partial T}{\partial x}+v\frac{\partial T}{\partial y}=\frac{1}{(\hat{\rho}c_p)_{nf}}\frac{\partial}{\partial y}\left(k_{nf}(T)\frac{\partial T}{\partial y}\right)+\frac{\breve{\mu}_{nf}}{(\hat{\rho}c_p)_{nf}}\left(4\left(\frac{\partial u}{\partial x}\right)^2+\left(\frac{\partial u}{\partial x}+\frac{\partial v}{\partial y}\right)^2\right), \tag{3}$$

The boundary conditions are:

$$\text{When } y\to 0\text{: } \frac{\partial u}{\partial y}=0, v=0, \text{ and } \frac{\partial T}{\partial y}=0, \tag{4}$$

$$\text{When } y\to h(t)\text{: } v_w=\frac{dh}{t}, \text{ and } T=T_H, \tag{5}$$

where $\tilde{p}$ is the fluid pressure, $C_{p_{nf}}$ is the effective specific heat of the nanofluid at constant pressure, u and v are the x and y directions velocities, $\hat{\rho}_{nf}$ is the density of the nanofluid, $\breve{\mu}_{nf}$ is the effective dynamic viscosity of the nanofluid, v_{nf} is the effective kinematic viscosity of the nanofluid, σ_{nf} is the electrical conductivity of the nanofluid, $k_{nf}(T)$ is the variable thermal conductivity of the nanofluid, B_0 is the electromagnetic induction, and φ is the angle of inclination of the applied magnetic field. The formulas for $\hat{\rho}_{nf}, \breve{\mu}_{nf}, v_{nf}, C_{p_{nf}}, \sigma_{nf}$ and $k_{nf}(T)$ can be seen as follows [14, 15], respectively:

$$\hat{\rho}_{nf}=\hat{\rho}_f(1-w)+\hat{\rho}_s w,\ \breve{\mu}_{nf}=\frac{\breve{\mu}_f}{(1-w)^{2.5}},\left(\hat{\rho}c_p\right)_{nf}=(1-w)\left(\hat{\rho}\,.c_p\right)_f+w\left(\hat{\rho}.c_p\right)_s,$$

$$\frac{k_{nf}}{k_f}=\frac{(k_s+2k_f)-2w(k_f-k_s)}{(k_s+2k_f)+2w(k_f-k_s)},\quad \frac{\sigma_{nf}}{\sigma_f}=1+\frac{3\left(\frac{\sigma_s}{\sigma_f}-1\right)w}{\left(\frac{\sigma_s}{\sigma_f}+2\right)-\left(\frac{\sigma_s}{\sigma_f}-1\right)w},\quad k_{nf}(T)=k_{nf}\left[1+\varepsilon\frac{T}{T_H}\right] \tag{6}$$

Where, σ_f is the base fluid, σ_s denote the solid nanoparticles, ε is the constant temperature profile, and w is the volume fraction of nanoparticles. The values of dimensionless parameters are introduced as follows:

$$\tau = \frac{y}{l(1-\varphi t)^{1/2}}, \quad u = \frac{\varphi x}{2(1-\varphi t)}\frac{d\bar{f}}{d\tau}, \quad v = \frac{\varphi x}{2(1-\varphi t)^{1/2}}\bar{f}, \quad T = \bar{g}\,T_H. \tag{7}$$

By incorporating the terms of Equation (7) into Equations (2) and (3), the resulting formulation is obtained as follows

$$\frac{d^4\bar{f}}{d\tau^4} - S.A_1.(1-w)^{2.5}\left[\tau\frac{d^3\bar{f}}{d\tau^3} + 3\frac{d^2\bar{f}}{d\tau^2} + \frac{d\bar{f}}{d\tau}\frac{d^2\bar{f}}{d\tau^2} - \bar{f}\frac{d^3\bar{f}}{d\tau^3}\right] - (1-w)^{2.5}HaA_4 sin^2(\varphi)\frac{d^2\bar{f}}{d\tau^2} = 0 \tag{8}$$

$$(1+\varepsilon\bar{g})\frac{d^2\bar{g}}{d\tau^2} + \varepsilon(\frac{d\bar{g}}{d\tau})^2 + \frac{S.PrA_2}{A_3}(\bar{f}\frac{d\bar{g}}{d\tau} - \tau\frac{d\bar{g}}{d\tau}) + \frac{PrEc}{A_3(1-w)^{2.5}}\left[\left(\frac{d^2\bar{f}}{d\tau^2}\right)^2 + 4\delta^2\left(\frac{d\bar{f}}{d\tau}\right)^2\right] = 0, \tag{9}$$

with:

$$A_1 = (1-w) + w.\frac{\hat{\rho}_s}{\hat{\rho}_f}, A_2 = (1-w) + w.\frac{(\hat{\rho}C_p)_s}{(\hat{\rho}C_p)_f}, A_3 = \frac{k_{nf}}{k_f} = \frac{(k_s+2k_f) - 2w(k_f-k_s)}{(k_s+2k_f) + 2w(k_f-k_s)},$$

$$A_4 = \left[1 + \frac{3\left(\frac{\sigma_s}{\sigma_f}-1\right)w}{\left(\frac{\sigma_s}{\sigma_f}+2\right) - \left(\frac{\sigma_s}{\sigma_f}-1\right)w}\right]. \tag{10}$$

The Squeeze, Prandtl, Eckert, and Hartmann numbers are introduced as:

$$S = \frac{\varphi l^2}{2v_f}, \quad P_r = \frac{\check{\mu}_f.(\hat{\rho}C_p)_f}{\hat{\rho}_f k_f}, \quad E_c = \frac{\hat{\rho}_f}{(\hat{\rho}C_p)_f}(\frac{\varphi x}{2(1-\varphi t)})^2, \quad Ha = \frac{2\sigma_f B_0^2 (h(t))^2}{\hat{\rho}_f \check{\mu}_f}, \quad \delta = \frac{1}{x}.$$

The modified boundary conditions are

$$\bar{f}(0) = 0,\ \frac{d^2\bar{f}(0)}{d\tau^2} = 0,\ \frac{d\bar{g}(0)}{d\tau} = 0,\ \frac{d\bar{f}(1)}{d\tau} = 0,\ \bar{f}(1) = 1,\ \frac{d\,\bar{g}(1)}{d\tau} = 1. \tag{11}$$

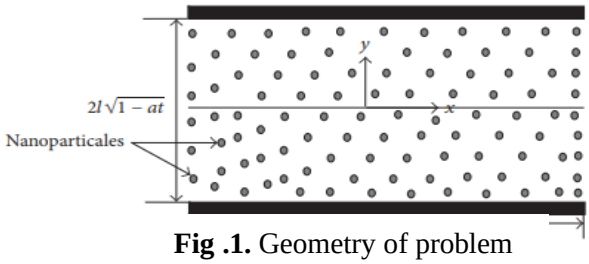

Fig .1. Geometry of problem

The physical quantities of the skin friction coefficient and Nusselt number are explained as:

$$\mathrm{C_f} = \frac{\check{\mu}_{nf}\,(\frac{\partial u}{\partial y})_{y=h(t)}}{\hat{\rho}_{nf}v_w^2}, \qquad N_u = \frac{-lk_{nf}(\frac{\partial T}{\partial y})_{y=h(t)}}{kT_H},$$

The expression derived from the terms of Equation (8) is given as follows:

$$C_f^* = \frac{l^2}{x^2(1-\varphi t)}R_{ex}C_f = A_1(1-w)^{2.5}\bar{f}''(1),\ N_u^* = \sqrt{1-\varphi t}\,N_u = -A_3\,\bar{g}(1).$$

3. Basic Idea of q-Homotopy Analysis Method

The technique known as q-homotopy analysis is based on topological homotopy and conventional perturbation. This method yields an approximate solution that approaches the exact solution. The non-linear differential equation can be expressed in the following way to show the fundamental ideas of q-HAM:

$$D(\bar{f}) + U(\bar{f}) + N(\bar{f}) - g(\tau) = 0,\ \tau \in \Omega \qquad \mathcal{K}(\bar{f}(\tau), \frac{d\bar{f}}{d\tau}) = 0\,; \tau \in \Gamma \tag{12}$$

Where the boundaries of the field Ω are displayed by Γ, $g(\tau)$ is a known analytic function, $\bar{f}$ denotes the unknown function, $\mathcal{K}$ denotes the boundary operator. D and U refer to the linear differential operator such that its order is less than D, N is the general non-linear differential operator. The

definition of the homotopy in the homotopy perturbation technique is $\bar{f}: \mathbb{R} \times [0, \frac{1}{n}] \to \mathbb{R}$ and constructed as

$$H(\bar{f}, q) = (1 - nq)[D(\bar{f}(\tau, q)) - D(\bar{f}_0)] - qhH(\tau)[D(\bar{f}(\tau)) + U(\bar{f}(\tau)) + N(\bar{f}(\tau)) - g(\tau)] = 0 \quad (13)$$

Here, $H(\tau)$ indicates a non-zero auxiliary function, $h \neq 0$ is an auxiliary parameter, $q \in [0, \frac{1}{n}], n \geq 1$ indicates the so-called embedded parameter, and $\bar{f}_0$ is an initial approximation of Equation (12) that precisely fulfills the boundary requirements. D is an acceptable auxiliary linear operator. The generic form of Equation (13) is as follows: when $q = 0$, $q = \frac{1}{n}$ is substituted, and $H(\tau) = 1$.

$$H(\bar{f}, 0) = D\left(\bar{f}(\tau, 0)\right) - D(\bar{f}_0), \quad (14)$$

$$H\left(\bar{f}, \frac{1}{n}\right) = \frac{h}{n}[D(\bar{f}(\tau, \frac{1}{n}) + U(\bar{f}(\tau, \frac{1}{n}) + +N(\bar{f}(\tau, \frac{1}{n})) - g(\tau)], \quad (15)$$

The deformation of topology is known as $\bar{f}(\tau, q)$ moves from $\bar{f}_0(\tau)$ to $\bar{f}(\tau)$ as moves from 0 to $\frac{1}{n}$.

As well, $[D(\bar{f}(\tau, q)) - D(\bar{f}_0)]$ and $[D(\bar{f}(\tau)) + U(\bar{f}(\tau)) + N(\bar{f}(\tau))]$ are referred to as homotopic. The power series that we obtain after solving Equation (13) is as follows:

$$\bar{f}(\tau, q) = \sum_{m=0}^{\infty} \bar{f}_m(\tau) q^m. \quad (16)$$

The correct solutions for the coefficients $\bar{f}_m(\tau)$ in Equation (16) can be obtained using the homotopy deformation equations [16]. Consequently, it is simple to get an approximate analytical solution to Equation (12) as

$$\bar{f}(\tau) = \lim_{q \to \frac{1}{n}} \bar{f}(\tau, q) = \sum_{m=0}^{\infty} \bar{f}_m(\tau) \left(\frac{1}{n}\right)^m, \quad (17)$$

where

$$\bar{f}_m(\tau) = \frac{1}{m!} \frac{d^m \bar{f}(\tau, q)}{dq^m}\Big|_{q=0}. \quad (18)$$

Equation (13) is derived m times concerning q with by putting $q = 0$ with the results by $m!$. The introduction of the vector is $\vec{\bar{f}}_m(\tau) = \{\bar{f}_0(\tau), \bar{f}_1(\tau), \bar{f}(\tau), \dots, \bar{f}_m(\tau)\}$. The m^{th}-order deformation equation can be defined by:

$$\bar{f}_m(\tau) = \delta_m \bar{f}_{m-1}(\tau) + hH(\tau)D^{-1}[R_m(\vec{\bar{f}}_{m-1}(\tau))], \quad (19)$$

where:

$$R_m(\vec{\bar{f}}_{m-1}(\tau)) = \frac{1}{(m-1)!} \frac{d^{m-1}[D\left(\bar{f}(\tau,q)\right) + U\left(\bar{f}(\tau,q)\right) + N\left(\bar{f}(\tau,q) - g(\tau)\right)]}{dq^{m-1}}\Big|_{q=0}, \quad (20)$$

And

$$\delta_m = \begin{cases} 0 & m \leq 1 \\ n & otherwise \end{cases}, \quad (21)$$

It is important to have linear boundary conditions for the proposed problem, the nonlinear Equation (19) is given $\bar{f}_m(\tau)$ for $m \geq 1$. In comparison to a typical HAM, the operator n allows for substantially faster convergence or even increases the probability of convergence. It should be noted that Equation (13) can be used to get the standard HAM for $n = 1$.

4. Padé Approximation

Padé Approximate is the best approximation of the function by a rational function**.** The following is the rational function defined by the power series:

$$\bar{f}(\tau) = \sum_{i}^{\infty} c_i x^i. \quad (22)$$

A rational function $\bar{f}(\tau)$ has a Padé approximation, which may be expressed in notation using the following form:

$$\bar{f}(\tau) = \frac{P_\ell(\tau)}{Q_\varkappa(\tau)}, \quad (23)$$

According to their definition, P_ℓ is a polynomial of degree at most ℓ and $Q_\varkappa$ is a polynomial of degree at most $\varkappa$ as

$$P_\ell(\tau) = \sum_{j=0}^{\ell} a_j \tau^j, \tag{24}$$

$$Q_\varkappa(\tau) = \sum_{i=0}^{\varkappa} b_i \tau^i, \tag{25}$$

Substituting Equations (22), (24), and (25) into Equation (23), yield

$$c_0\tau^0 + c_1\tau^1 + c_2\tau^2 + \cdots = \frac{a_0\tau^0 + a_1\tau^1 + a_2\tau^2 + a_3\tau^3 + \cdots + a_\ell\tau^\ell}{b_0\tau^0 + b_1\tau^1 + b_2\tau^2 + b_3\tau^3 + \cdots + b_\varkappa\tau^\varkappa} + O\left(\tau^{\ell+\varkappa+1}\right), \tag{26}$$

Where $b_0 = 1$, Equation (26) is rearranged to take on the form

$$(c_0\tau^0 + c_1\tau^1 + c_2\tau^2 + \cdots)(b_0\tau^0 + b_1\tau^1 + b_2\tau^2 + b_3\tau^3 + \cdots + b_\varkappa\tau^\varkappa) = a_0\tau^0 + a_1\tau^1 + a_2\tau^2 + a_3\tau^3 + \cdots + a_\ell\tau^\ell + O\left(\tau^{\ell+\varkappa+1}\right), \tag{27}$$

The following equations can be obtained from Equation (27).

$$c_0 = a_0,$$

$$c_0 b_1 + c_1 = a_1,$$

$$c_0 b_2 + c_1 b_1 + c_2 = a_2,$$

$$\vdots$$

$$c_0 b_\varkappa + c_1 b_{\varkappa-1} + c_2 b_{\varkappa-2} + \cdots + c_\varkappa = a_\ell.$$

And

$$c_{\ell+1} + c_\ell b_1 + c_{\ell-1} b_2 + \cdots + c_{\ell-\varkappa+1} b_\varkappa = 0,$$

$$c_{\ell+2} + c_{\ell+1} b_1 + c_\ell b_2 + \cdots + c_{\ell-\varkappa+2} b_\varkappa = 0,$$

$$\vdots$$

$$c_{\ell+\varkappa} + c_{\ell+\varkappa-1} b_1 + c_{\ell+\varkappa-2} b_2 + \cdots + c_\ell b_\varkappa = 0.$$

The Padé approximation of the rational function [17] can be obtained by solving the above system; we obtain the unknown values that are substituted into Equation (26).

5. The Basic Idea of LTCP-q-HAM

This section illustrates the hybrid methodology that combines the convolution theory-supported Laplace transform with the q-homotopy analysis method and Padé approximation. By rewriting Equation (12) assuming that $D = \frac{d^n}{d\tau^n}$ as the operator's definition, which is as follows:

Considering the effects of the Laplace transforms on both sides of Equation (28), as follows:

$$\frac{d^n \bar{f}(\tau)}{d\tau^n} + U\left(\bar{f}(\tau)\right) + N\left(\bar{f}(\tau)\right) - g(\tau) = 0 \tag{28}$$

$$\mathcal{L}\left[\frac{d^n \bar{f}(\tau)}{d\tau^n} + U\left(\bar{f}(\tau)\right) + N\left(\bar{f}(\tau)\right) - g(\tau)\right] = 0, \tag{29}$$

From the properties of the Laplace transform for Equation (29), the following outcomes are obtained:

$$s^n \mathcal{L}\left[\bar{f}(\tau)\right] - \sum_{\omega=0}^{n-1} s^{n-\omega-1} \bar{f}^{(\omega)}(0) + \mathcal{L}\left[U\left(\bar{f}(\tau)\right) + N\left(\bar{f}(\tau)\right) - g(\tau)\right] = 0, \tag{30}$$

Rearranging Equation (30) yield in:

$$\mathcal{L}\left[\bar{f}(\tau)\right] - \frac{1}{s^n}\sum_{\omega=0}^{n-1} s^{n-\omega-1} \bar{f}^{(\omega)}(0) + \frac{1}{s^n}\mathcal{L}\left[U\left(\bar{f}(\tau)\right) + N\left(\bar{f}(\tau)\right) - g(\tau)\right] = 0, \tag{31}$$

The Laplace transform properties can be applied, substituting $\frac{1}{s^n} = \frac{\mathcal{L}[\tau^{n-1}]}{(n-1)!}$ in Equation (31); we get

$$\mathcal{L}\left[\bar{f}(\tau)\right] - \frac{1}{(n-1)!}\mathcal{L}[\tau^{n-1}]\sum_{\omega=0}^{n-1} s^{n-\omega-1}\bar{f}^{(\omega)}(0) + \frac{1}{(n-1)!}\mathcal{L}[\tau^{n-1}] \times \mathcal{L}\left[U\left(\bar{f}(\tau)\right) + N\left(\bar{f}(\tau)\right) - g(\tau)\right] = 0, \quad (32)$$

Where Equation (32) can be written as follows:

$$\mathcal{L}\left[\bar{f}(\tau)\right] - \frac{1}{(n-1)!}\mathcal{L}[\tau^{n-1}]\sum_{\omega=0}^{n-1} s^{n-\omega-1}\bar{f}^{(\omega)}(0) + \mathcal{L}\left[\frac{\tau^{n-1}}{(n-1)!} * \left(U\left(\bar{f}(\tau)\right) + N\left(\bar{f}(\tau)\right) - g(\tau)\right)\right] = 0, \quad (33)$$

The operation * is defined by:

- $\mathcal{L}[\bar{f}(\tau) * \bar{g}(\tau)] = \mathcal{L}[\bar{f}(\tau) \times \bar{g}(\tau)]$,
- $\bar{f}(\tau) * \bar{g}(\tau) = \int_0^\tau \bar{f}(\tau-\xi)\bar{g}(\xi)d\xi$,

By applying the convolution theory of Equation (33), the following results can be become:

$$\mathcal{L}\left[\bar{f}(\tau)\right] - \frac{\mathcal{L}[\tau^{n-1}]}{(n-1)!}\sum_{\omega=0}^{n-1} s^{n-\omega-1}\bar{f}^{(\omega)}(0) + \mathcal{L}[\int_0^\tau \frac{(\tau-\xi)^{n-1}}{(n-1)!}(U(\bar{f}(\tau)) + N(\bar{f}(\tau)) - g\,(\tau)]|_{\tau=\xi}d\xi = 0. \quad (34)$$

Hence, the nonlinear operator can be displayed as follows:

$$B\left[\bar{f}(\tau,q)\right] = \mathcal{L}\left[\bar{f}(\tau)\right] - \frac{\mathcal{L}[\tau^{n-1}]}{(n-1)!}\sum_{\omega=0}^{n-1} s^{n-\omega-1}\bar{f}^{(\omega)}(0) + \mathcal{L}[\int_0^\tau \frac{(\tau-\xi)^{n-1}}{(n-1)!} \times (U\left(\bar{f}(\tau)\right) + N(\bar{f}(\tau)) - g\,(\tau))|_{\tau=\xi}d\xi\,]. \quad (35)$$

Now, taking the first term of Equation (19) Laplace transforms the results into are

$$\mathcal{L}[\bar{f}_m(\tau) - \delta_m\,\bar{f}_{m-1}(\tau)] = hqH(\tau)[R_m(\vec{\bar{f}}_{m-1}(\tau))], \quad (36)$$

The above equation, after taking the inverse of the Laplace transform, has the following formula:

$$\bar{f}_m(\tau) = \delta_m\,\bar{f}_{m-1}(\tau) + hqH(\tau)\mathcal{L}^{-1}[R_m(\vec{\bar{f}}_{m-1}(\tau))], \quad (37)$$

where,

$$R_m(\vec{\bar{f}}_{m-1}(\tau)) = \frac{1}{(m-1)!}\frac{d^{m-1}(B\left[\bar{f}(\tau,q)\right])]}{dq^{m-1}}\bigg|_{q=0},$$

Pade´ approximation $P_\varkappa^\ell$ of Equation (37)

$$P_\varkappa^\ell\left[\bar{f}_m(\tau)\right] = \delta_m\,\bar{f}_{m-1}(\tau) + hqH(\tau)\mathcal{L}^{-1}[R_m(\vec{\bar{f}}_{m-1}(\tau))], \quad (38)$$

6. The Applications of LTCP-q-HAM

The nonlinear ordinary differential Equations (9) and (10) are solved by LTCP-q-HAM and q-HAM to obtain an approximate analytical solution. The following is an explanation of these applications:

$$\frac{d^4\bar{f}}{d\tau^4} - S.A_1.(1-w)^{2.5}\left[\tau\frac{d^3\bar{f}}{d\tau^3} + 3\frac{d^2\bar{f}}{d\tau^2} + \frac{d\bar{f}}{d\tau}\frac{d^2\bar{f}}{d\tau^2} - \bar{f}\frac{d^3\bar{f}}{d\tau^3}\right] - (1-w)^{2.5}HaA_4sin^2(\varphi)\frac{d^2\bar{f}}{d\tau^2} = 0 \quad (39)$$

$$(1+\varepsilon\bar{g})\frac{d^2\bar{g}}{d\tau^2} + \varepsilon(\frac{d\bar{g}}{d\tau})^2 + \frac{S.PrA_2}{A_3}(\bar{f}\frac{d\bar{g}}{d\tau} - \tau\frac{d\bar{g}}{d\tau}) + \frac{PrEc}{A_3(1-w)^{2.5}}\left[\left(\frac{d^2\bar{f}}{d\tau^2}\right)^2 + 4\delta^2\left(\frac{d\bar{f}}{d\tau}\right)^2\right] = 0, \quad (40)$$

The assumptions of the initial conditions are:

$$\bar{f}_0(\tau) = \Gamma_0 + \Gamma_1\tau + \Gamma_2\frac{\tau^2}{2!} + \Gamma_3\frac{\tau^3}{2!}, \quad (41)$$

$$\bar{g}_0(\tau) = \Psi_0 + \Psi_1\tau, \quad (42)$$

Where $\bar{f}(0) = \Gamma_0,\ \bar{f}'(0) = \Gamma_1\ ,\bar{f}''(0) = \Gamma_2, \bar{f}'''(0) = \Gamma_3,\quad \bar{g}\,(0) = \Psi_0,\ \bar{g}'(0) = \Psi_1,$

By using Equation (11) and Equations (41) and (42) the groups of initial condition are readily found, as follows:

$$\bar{f}_0(\tau) = \Gamma_1\tau + \Gamma_3\frac{\tau^3}{3!}, \tag{43}$$

$$\bar{g}_0(\tau) = \Psi_0, \tag{44}$$

From Adomain polynomials, a nonlinear operator is defined as follows:

$$R_m(\vec{\bar{f}}_{m-1}(\tau)) = \frac{d^4\bar{f}_{m-1}}{d\tau^4} - S.A_1.(1-w)^{2.5}[\tau\frac{d^3\bar{f}_{m-1}}{d\tau^3} + 3\frac{d^2\bar{f}_{m-1}}{d\tau^2} + \sum_{z=0}^{m-1}\sum_{s=0}^{z}\frac{d}{d\tau}\bar{f}_s\frac{d^2}{d\tau^2}\bar{f}_{m-1-z}) -$$

$$\sum_{z=0}^{m-1}\sum_{s=0}^{z}\bar{f}_s\frac{d^3}{d\tau^3}\bar{f}_{m-1-z}] - (1-w)^{2.5}HaA_4sin^2(\varphi)\frac{d^2\bar{f}_{m-1}}{d\tau^2}, \quad m = 1,2,\ldots \tag{45}$$

$$R_m\left(\vec{\bar{g}}_{m-1}(\tau)\right) = (1+\varepsilon\bar{g})\frac{d^2\bar{g}_{m-1}}{d\tau^2} + \varepsilon(\sum_{z=0}^{m-1}\frac{d}{d\tau}\bar{g}_{m-1-z})^2 + \frac{S.PrA_2}{A_3}(\sum_{z=0}^{m-1}\sum_{s=0}^{z}\bar{f}_s\frac{d}{d\tau}\bar{g}_{m-1-z} -$$

$$\tau\frac{d\bar{g}_{m-1}}{d\tau}) + \frac{PrEc}{A_3(1-w)^{2.5}}\left[\left(\sum_{z=0}^{m-1}\frac{d^2}{d\tau^2}\bar{f}_{m-1-z}\right)^2 + 4\delta^2\left(\sum_{z=0}^{m-1}\frac{d}{d\tau}\bar{f}_{m-1-z}\right)^2\right], \ m = 1,2,\ldots \tag{46}$$

Now, Equations (8) and (9) can be solved to get:

$$\bar{f}_m(\tau) = \delta_m\bar{f}_{m-1}(\tau) + hH(\tau)\int_0^\tau\int_0^\tau\int_0^\tau\int_0^\tau[\frac{d^4\bar{f}_{m-1}}{d\tau^4} - S.A_1.(1-w)^{2.5}[\tau\frac{d^3\bar{f}_{m-1}}{d\tau^3} + 3\frac{d^2\bar{f}_{m-1}}{d\tau^2}$$

$$+\sum_{z=0}^{m-1}\sum_{s=0}^{z}\frac{d}{d\tau}\bar{f}_s\frac{d^2}{d\tau^2}\bar{f}_{m-1-z}) - \sum_{z=0}^{m-1}\sum_{s=0}^{z}\bar{f}_s\frac{d^3}{d\tau^3}\bar{f}_{m-1-z}] - (1-w)^{2.5}$$

$$HaA_4sin^2(\varphi)\frac{d^2\bar{f}_{m-1}}{d\tau^2}]d\tau, \quad m = 1,2,\ldots \tag{47}$$

$$\bar{g}_m(\tau) = \delta_m\bar{g}_{m-1}(\tau) + hH(\tau)\int_0^\tau\int_0^\tau\{(1+\varepsilon\bar{g})\frac{d^2\bar{g}_{m-1}}{d\tau^2} + \varepsilon(\sum_{z=0}^{m-1}\frac{d}{d\tau}\bar{g}_{m-1-z})^2 +$$

$$\frac{S.PrA_2}{A_3}(\sum_{z=0}^{m-1}\sum_{s=0}^{z}\bar{f}_s\frac{d}{d\tau}\bar{g}_{m-1-z} - \tau\frac{d\bar{g}_{m-1}}{d\tau}) + \frac{PrEc}{A_3(1-w)^{2.5}}[\left(\sum_{z=0}^{m-1}\frac{d^2}{d\tau^2}\bar{f}_{m-1-z}\right)^2 +$$

$$4\delta^2\left(\sum_{z=0}^{m-1}\frac{d}{d\tau}\bar{f}_{m-1-z}\right)^2]\}d\tau, \quad m = 1,2,\ldots \tag{48}$$

The resulting solution has several iterations of analytical solutions that can be introduced by the following:

$$\bar{f}_1(\tau) = (-0.04166666665hHaA_4sin^2(\varphi)(1-w)^{2.5}\Gamma_3 - 0.04166666665hSA_1(1-w)^{2.5}\Gamma_1\Gamma_3 -$$

$$0.1250000000hSA_1(1-w)^{2.5}\Gamma_3)\tau^4 - 0.008333333336hSA_1(1-w)^{2.5}\Gamma_3^2\tau^5.$$

$$\bar{f}_2(\tau) = (-0.04166666665nhHaA_4sin^2(\varphi)(1-w)^{2.5}\Gamma_3$$
$$- 0.04166666665nhSA_1(1-w)^{2.5}\Gamma_1\Gamma_3 -$$

$$0.1250000000nhSA_1(1-w)^{2.5}\Gamma_3 - 0.1250000000h^2SA_1(1-w)^{2.5}\Gamma_3$$
$$- 0.04166666665h^2HaA_4$$

$sin^2(\varphi)(1-w)^{2.5}\Gamma_3 - 0.04166666666h^2SA_1(1-w)^{2.5}\Gamma_1\Gamma_3)\tau^4(-0.008333333336nhSA_1$

$(1-w)^{2.5}\Gamma_3^2 - 0.0083333333336h^2SA_1(1-w)^{2.5}\Gamma_3^2)\tau^5 + (0.02083333334h^2S^2A_1^2\Gamma_3 +$

$0.01388888888h^2Ha^2A_4^2sin^4(\varphi)\Gamma_3w^2 - \cdots$

$\vdots$

$$\bar{g}_1(\tau) = \frac{1}{A_3(1-w)^{2.5}}[(2hP_rE_c\delta^2\Gamma_1^2 + 0.5hP_rE_c\delta^2\Gamma_3^2)\tau^2 + 1.333333333hP_rE_c\delta^2\Gamma_1\Gamma_3\tau^3 +$$

$$0.3333333333hP_rE_c\delta^2\Gamma_3^2\tau^4].$$

$$\bar{g}_2(\tau) = \frac{1}{A_3(1-w)^{2.5}}(2nhP_rE_c\delta^2\Gamma_1^2 + 0.5nhP_rE_c\Gamma_3^2 + 0.5h^2P_rE_c\varepsilon\Psi_0\Gamma_3^2 + 2h^2P_rE_c\varepsilon\Psi_0\Gamma_1^2 +$$

$$0.5h^2P_rE_c\Gamma_3^2 + 2h^2P_rE_c\delta^2\Gamma_1^2)\tau^2 + \frac{1}{A_3(1-w)^{2.5}}(1.333333333nhP_rE_c\delta^2\Gamma_1\Gamma_3 +$$

$$1.333333333h^2P_rE_c\delta^2\Gamma_1\Gamma_3 + 1.333333333h^2P_rE_c\delta^2\varepsilon\Psi_0\Gamma_1\Gamma_3)\tau^3 + \frac{0.33333333nhP_rE_c\delta^2\Gamma_3^2}{A_3(1-w)^{2.5}}$$

$$-\frac{0.08333333332h^2SP_r^2E_cA_2\Gamma_3^2}{A_3^2(1-w)^{2.5}} - \frac{0.08333333330h^2P_rE_cA_4Hasin^2(\varphi)\Gamma_3^2}{A_3} -$$

$$\frac{0.08333333330h^2SP_rE_cA_1\Gamma_3^2}{A_3} + \frac{0.333333332h^2SP_r^2E_c\delta^2A_2\Gamma_1^3}{A_3^2(1-w)^{2.5}} + \cdots.$$

The remaining iterative components, $\bar{f}_m(\tau)$ and $\bar{g}_m(\tau)$, $m = 3,4,5,6,\ldots$ can be acquired by resemblance. The following is the formulation for the series solution by q-HAM:

$$\left.\begin{aligned}\bar{f}(\tau,n;h) \cong \bar{f}_m(\tau,n;h) = \textstyle\sum_{i=0}^{m} u_i(\tau,n;h)\left(\frac{1}{n}\right)^i,\ n = 1,2,\ldots\\ \bar{g}(\tau,n;h) \cong \bar{g}_m(\tau,n;h) = \textstyle\sum_{i=0}^{m} u_i(\tau,n;h)\left(\frac{1}{n}\right)^i,\ n = 1,2,\ldots\end{aligned}\right\} \quad (49)$$

By using LTCP-q-HAM to find the analytical approximate solution by taking the Laplace transform to both sides of Equations (8) and (9), become

$$\mathcal{L}\left[\frac{d^4\bar{f}}{d\tau^4}\right] - S.A_1.(1-w)^{2.5}\mathcal{L}\left[\tau\frac{d^3\bar{f}}{d\tau^3} + 3\frac{d^2\bar{f}}{d\tau^2} + \frac{d\bar{f}}{d\tau}\frac{d^2\bar{f}}{d\tau^2} - \bar{f}\frac{d^3\bar{f}}{d\tau^3}\right] - (1-w)^{2.5}HaA_4sin^2(\varphi)$$

$$\mathcal{L}\left[\frac{d^2\bar{f}}{d\tau^2}\right] = 0, \quad (50)$$

$$\mathcal{L}\left[\frac{d^2\bar{g}}{d\tau^2}\right] + \mathcal{L}\{\varepsilon\bar{g}\frac{d^2\bar{g}}{d\tau^2} + \varepsilon\left(\frac{d\bar{g}}{d\tau}\right)^2 + \frac{S.PrA_2}{A_3}(\bar{f}\frac{d\bar{g}}{d\tau} - \tau\frac{d\bar{g}}{d\tau}) + \frac{PrEc}{A_3(1-w)^{2.5}}[\left(\frac{d^2\bar{f}}{d\tau^2}\right)^2 + 4\delta^2\left(\frac{d\bar{f}}{d\tau}\right)^2]\} = 0, \quad (51)$$

By implementing the differentiation property of the Laplace transform with the help of the initial condition from Equations (50) and (51), we get

$$\mathcal{L}[\bar{f}] - \left(\frac{\Gamma_1 s^2 + \Gamma_3}{s^4}\right) - \frac{1}{s^4}\mathcal{L}[S.A_1.(1-w)^{2.5}\left(\tau\frac{d^3\bar{f}}{d\tau^3} + 3\frac{d^2\bar{f}}{d\tau^2} + \frac{d\bar{f}}{d\tau}\frac{d^2\bar{f}}{d\tau^2} - \bar{f}\frac{d^3\bar{f}}{d\tau^3}\right) - (1-w)^{2.5}HaA_4 sin^2(\varphi)\frac{d^2\bar{f}}{d\tau^2}] = 0, \quad (52)$$

$$\mathcal{L}[\bar{g}\,] - \frac{\Psi_0}{s} + \frac{1}{s^2}\mathcal{L}\{\varepsilon\bar{g}\frac{d^2\bar{g}}{d\tau^2} + \varepsilon\left(\frac{d\bar{g}}{d\tau}\right)^2 + \frac{S.PrA_2}{A_3}(\bar{f}\frac{d\bar{g}}{d\tau} - \tau\frac{d\bar{g}}{d\tau}) + \frac{PrEc}{A_3(1-w)^{2.5}}[\left(\frac{d^2\bar{f}}{d\tau^2}\right)^2 + 4\delta^2\left(\frac{d\bar{f}}{d\tau}\right)^2]\} = 0, \quad (53)$$

From the Laplace transform's properties substituting $\frac{1}{s^4} = \frac{1}{3!}\mathcal{L}[\tau^3]$ and $\frac{1}{s^2} = \frac{1}{1!}\mathcal{L}[\tau]$ in Equations (52) and (53) respectively, we get the following results:

$$\mathcal{L}[\bar{f}] - \left(\frac{\Gamma_1 s^2 + \Gamma_3}{s^4}\right) - \frac{1}{3!}\mathcal{L}[\tau^3] \times \mathcal{L}[S.A_1.(1-w)^{2.5}\left(\tau\frac{d^3\bar{f}}{d\tau^3} + 3\frac{d^2\bar{f}}{d\tau^2} + \frac{d\bar{f}}{d\tau}\frac{d^2\bar{f}}{d\tau^2} - \bar{f}\frac{d^3\bar{f}}{d\tau^3}\right) - (1-w)^{2.5} HaA_4 sin^2(\varphi)\frac{d^2\bar{f}}{d\tau^2}] = 0, \quad (54)$$

$$\mathcal{L}[\bar{g}\,] - \frac{\Psi_0}{s} + \frac{1}{1!}\mathcal{L}[\tau] \times \mathcal{L}\{\varepsilon\bar{g}\frac{d^2\bar{g}}{d\tau^2} + \varepsilon\left(\frac{d\bar{g}}{d\tau}\right)^2 + \frac{S.PrA_2}{A_3}(\bar{f}\frac{d\bar{g}}{d\tau} - \tau\frac{d\bar{g}}{d\tau}) + \frac{PrEc}{A_3(1-w)^{2.5}}[\left(\frac{d^2\bar{f}}{d\tau^2}\right)^2 + 4\delta^2\left(\frac{d\bar{f}}{d\tau}\right)^2]\} = 0, \quad (55)$$

The convolution theory concept uses the last terms of Equation (54) and Equation (55), the outcome can be obtained following:

$$\mathcal{L}[\bar{f}] - \left(\frac{\Gamma_1 s^2 + \Gamma_3}{s^4}\right) - \mathcal{L}[\frac{1}{3!}\tau^3 * (S.A_1.(1-w)^{2.5}\left(\tau\frac{d^3\bar{f}}{d\tau^3} + 3\frac{d^2\bar{f}}{d\tau^2} + \frac{d\bar{f}}{d\tau}\frac{d^2\bar{f}}{d\tau^2} - \bar{f}\frac{d^3\bar{f}}{d\tau^3}\right) - (1-w)^{2.5}HaA_4 sin^2(\varphi)\frac{d^2\bar{f}}{d\tau^2})] = 0, \quad (56)$$

$$\mathcal{L}[\bar{g}\,] - \frac{\Psi_0}{s} + \mathcal{L}\{\tau * (\varepsilon\bar{g}\frac{d^2\bar{g}}{d\tau^2} + \varepsilon\left(\frac{d\bar{g}}{d\tau}\right)^2 + \frac{S.PrA_2}{A_3}(\bar{f}\frac{d\bar{g}}{d\tau} - \tau\frac{d\bar{g}}{d\tau}) + \frac{PrEc}{A_3(1-w)^{2.5}}[\left(\frac{d^2\bar{f}}{d\tau^2}\right)^2 + 4\delta^2\left(\frac{d\bar{f}}{d\tau}\right)^2])\} = 0, \quad (57)$$

From taking the inverse Laplace transform for both sides of Equations (56) and (57) and from q-HAM the following results are:

$$\bar{f}_m(\tau) = \delta_m\bar{f}_{m-1}(\tau) + h\mathcal{L}^{-1}\left(\mathcal{L}[\bar{f}_{m-1}] - \left(1 - \frac{1}{n}\delta_m\right)\left(\frac{\Gamma_1 s^2 + \Gamma_3}{s^4}\right)\right) - \frac{h}{3!}\int_0^\tau((\tau-\xi)^3\,[S.A_1(1-w)^{2.5}.(\tau\frac{d^3\bar{f}}{d\tau^3} + 3\frac{d^2\bar{f}}{d\tau^2} + \sum_{z=0}^{m-1}\sum_{s=0}^{z}\frac{d}{d\tau}\bar{f}_s\frac{d^2}{d\tau^2}\bar{f}_{m-1-z}) - \sum_{z=0}^{m-1}\sum_{s=0}^{z}\bar{f}_s\frac{d^3}{d\tau^3}\bar{f}_{m-1-z}] -$$

$$(1-w)^{2.5}HaA_4sin^2(\varphi)\frac{d^2\bar{f}}{d\tau^2})]\Big|_{\tau=\xi})d\xi, \quad (58)$$

$$\bar{g}_m(\tau)=\delta_m\bar{g}_{m-1}(\tau)+h\mathcal{L}^{-1}\left(\mathcal{L}[\bar{g}_{m-1}]-\left(1-\frac{1}{n}\delta_m\right)\left(\frac{\Psi_0}{s}\right)\right)+\int_0^\tau((\tau-$$
$$\xi)[\sum_{z=0}^{m-1}\sum_{s=0}^{z}\varepsilon\bar{g}_s\frac{d^2}{d\tau^2}\bar{g}_{m-1-z}$$
$$+\varepsilon(\sum_{z=0}^{m-1}\frac{d}{d\tau}\bar{g}_{m-1-z})^2+\frac{S.PrA_2}{A_3}\left(\sum_{z=0}^{m-1}\sum_{s=0}^{z}\bar{f}_s\frac{d}{d\tau}\bar{g}_{m-1-z}-\tau\frac{d\bar{g}_{m-1}}{d\tau}\right)+\frac{PrEc}{A_3(1-w)^{2.5}}$$
$$[\left(\sum_{z=0}^{m-1}\frac{d^2}{d\tau^2}\bar{f}_{m-1-z}\right)^2+4\delta^2\left(\sum_{z=0}^{m-1}\frac{d}{d\tau}\bar{f}_{m-1-z}\right)^2]\Big|_{\tau=\xi})d\xi, \quad (59)$$

$$\bar{f}_1(\tau)=\Gamma_1\tau+\frac{1}{n}[(0.5h\Gamma_3+0.5\Gamma_3n)\tau^2-0.1666666667h\Gamma_3\tau^3$$
$$+(-0.04166666665hHaA_4sin^2(\varphi)$$
$$(1-w)^{2.5}\Gamma_3-0.04166666665hSA_1(1-w)^{2.5}\Gamma_1\Gamma_3-0.125hSA_1(1-w)^{2.5}\Gamma_3)\tau^4-$$
$$0.008333333350hSA_1(1-w)^{2.5}\Gamma_3^2\tau^5.$$

$$\bar{f}_2(\tau)=\Gamma_1\tau+\frac{1}{n^2}[(0.5000000001h^2\Gamma_3+nh\Gamma_3+0.5000000000n^2\Gamma_3)\tau^2$$
$$+(-0.166666667h^2\Gamma_3$$
$$-0.3333333334nh\Gamma_3)\tau^3+(-0.008333333331h^2HaA_4sin^2(\varphi)(1-w)^{2.5}\Gamma_3-$$
$$0.008333333330nhHaA_4sin^2(\varphi)(1-w)^{2.5}\Gamma_3-0.008333333331h^2SA_1(1-w)^{2.5}\Gamma_1\Gamma_3-$$
$$0.008333333330nhSA_1(1-w)^{2.5}\Gamma_1\Gamma_3-0.2500000000h^2SA_1(1-w)^{2.5}\Gamma_3-$$
$$0.2500000000nhSA_1(1-w)^{2.5}\Gamma_3)\tau^4+(0.0008333333350h^2HaA_4sin^2(\varphi)(1-w)^{2.5}\Gamma_3-$$
$$0.002500000002h^2SA_1(1-w)^{2.5}\Gamma_3^2-\cdots$$

⋮

Now, take the Pade´s approximation at the fourth iteration we get:

$$P_0^7\left(\bar{f}_4(\tau)\right)=1.445131944\tau-0.001273801303\tau^2-0.3881113444\tau^3-0.004971623653\tau^4$$
$$-0.04782596097\tau^5-0.001410484899\tau^6-0.001538728431\tau^7.$$

$$\bar{g}_1(\tau)=\Psi_0+\frac{1}{nA_3(1-w)^{2.5}}[(2hP_rE_c\delta^2\Gamma_1^2+0.5hP_rE_c\delta^2\Gamma_3^2)\tau^2+1.333333334hP_rE_c\delta^2\Gamma_1\Gamma_3\tau^3$$
$$+$$
$$0.3333333330hP_rE_c\delta^2\Gamma_3^2\tau^4].$$

$$\bar{g}_2(\tau)=\Psi_0+\frac{1}{A_3^2(1-w)^{2.5}n^2}[(2h^2P_rE_c\delta^2\varepsilon\Psi_0A_3\Gamma_1^2+2h^2P_rE_c\delta^2A_3\Gamma_1^2+4nhP_rE_c\delta^2A_3\Gamma_1^2+$$

$$0.5h^2P_rE_c\varepsilon\Psi_0A_3\Gamma_3^2 + 1.5h^2P_rE_cA_3\Gamma_3^2 + nhP_rE_cA_3\Gamma_3^2)\tau^2 + (1.333333334h^2P_rE_c\delta^2\varepsilon\Psi_0A_3\Gamma_1\Gamma_3$$
$$+$$
$$2.666666668h^2P_rE_c\delta^2A_3\Gamma_1\Gamma_3 + 2.666666668nhP_rE_c\delta^2A_3\Gamma_1\Gamma_3 - 0.3333333334h^2P_rE_c\delta^2A_3\Gamma_3^2)\tau^3 +$$
$$(-0.08333333330h^2P_rE_cA_3A_4Hasin^2(\varphi)(1-w)^{2.5}\Gamma_3^2$$
$$- 0.08333333330h^2P_rE_cSA_1A_3Hasin^2(\varphi)$$
$$(1-w)^{2.5}\Gamma_1\Gamma_3^2 - 0.2499999999h^2P_rE_cSA_1A_3(1-w)^{2.5}\Gamma_3^2 + 0.3333333330h^2P_r^2E_c\delta^2SA_2\Gamma_1^3$$
$$- \cdots$$

Now, take Pade´s approximation at the fourth iteration we get:

$$P_0^7\left(\bar{f}_4(\tau)\right) = 1.276801013 + 0.1328106758\tau^2 - 0.1198231839\tau^3 - 0.03499795754\tau^4 -$$
$$0.1810308875\tau^5 - 0.02213432925\tau^6 - 0.05162533074\tau^7.$$

6. Results and Discussions

The impact of an inclined magnetic field and variable thermal conductivity on heat transfer of squeezing unsteady ferrofluid flow with nanoparticle materials Au, and Fe_3O_4 has been examined, as well as different values for $S, Ha, \delta, w, \varepsilon, P_r, E_c$, and φ for velocity and temperature distributions. Tables (2) and (3) the convergence of values Γ_1,and Γ_3 for nanoparticle materials Au, and Fe_3O_4 is illustrated. These tables show that the values of Γ_1 are constant for q-HAM at the fourth approximation and for LTCP-q-HAM at the third approximation, while the values of Γ_3 are constant for q-HAM at the fifth approximation but LTCP-q-HAM at the third approximation, meaning that the constants for LTCP-q-HAM are better and converge to the values of BVP4C. From Tables (4) and (5), it can be observed that the convergence of Ψ_0, where the new technique appears converges to the numerical approximation of q-HAM. The effect of the Nusselt number for nanoparticle materials is displayed in Tables (6)-(8). From these tables, it can be seen that the values of the Nusselt number for LTCP-q-HAM are more accurate than for q-HAM when $\varphi = 5°$and $\varphi = 12°$ and it can be observed that the values of the BVP4C for $\varphi = 5°$ for all materials are equal; which means the effect of the materials is similar, while the values of the BVP4C for $\varphi = 12°$ are different meaning, these materials have the same impact for $0 \le \varphi \le 12°$ while inverse occurs when $\varphi \ge 12°$ Tables (9)-(11). These tables demonstrated the increasing of physical parameters led to an increment of the skin friction coefficient as well as the optimization of results through LTCP-q-HAM.

Table 2. The convergence of Γ_1, Γ_3 for material Au when $n = 2, h = -2, S = 0.5, Ha = 10, \delta = 0.1, w = 0, \varepsilon = 0, P_r = 0.1, E_c = 0.01, \varphi = 5°$.

Approximates	**q-HAM**		**LTCP-q-HAM**		**BVP4C**	
	Γ_1	Γ_3	Γ_1	Γ_3	Γ_1	Γ_3
1 order	1.759799	-1.272649	1.431209	-1.690339	1.493209	-3.092849
2 orders	1.742052	-1.232354	1.432153	-2.204750	1.485231	-3.092581
3 orders	1.741697	-1.231622	1.457024	-2.484290	1.485231	-3.092581
4 orders	1.741707	-1.231640	1.457024	-2.484290	1.485231	-3.092581
5 orders	1.741707	-1.231641	1.457024	-2.484290	1.485245	-3.092593
6 orders	1.741707	-1.231641	1.457024	-2.484290	1.485245	-3.092593

Table 3. The convergence of Γ_1, Γ_3 for material $Fe_3O_4$when $n = 2, h = -2, S = 0.5, Ha = 10, \delta = 0.1, w = 0, \varepsilon = 0, P_r = 0.1, E_c = 0.01, \varphi = 5°$.

Approximates	**q-HAM**		**LTCP-q-HAM**		**BVP4C**	
	Γ_1	Γ_3	Γ_1	Γ_3	Γ_1	Γ_3
1 order	1.759799	-1.272649	1.431209	-1.690339	1.493209	-3.092849
2 orders	1.742052	-1.232354	1.432153	-2.204750	1.485231	-3.092581
3 orders	1.741697	-1.231622	1.457024	-2.484290	1.485231	-3.092581

4 orders	1.741707	-1.231640	1.457024	-2.484290	1.485231	-3.092581
5 orders	1.741707	-1.231641	1.457024	-2.484290	1.485245	-3.092593
6 orders	1.741707	-1.231641	1.457024	-2.484290	1.485245	-3.092593

Table 4. The convergence of Ψ_0 for material Au when $n = 2, h = -2, S = 0.5, Ha = 10, \delta = 0.1, w = 0, \varepsilon = 0, P_r = 0.1, E_c = 0.01, \varphi = 5^\circ$

Approximates	q-HAM	LTCP-q-HAM	BVP4C
1 order	1.000847	1.001446	1.000786
2 orders	1.001086	1.000058	1.000744
3 orders	1.001167	1.000732	1.000744
4 orders	1.001177	1.000686	1.000744
5 orders	1.001178	1.000686	1.000744
6 orders	1.001178	1.000686	1.000744

Table 5. The convergence of Ψ_0 for material Fe_3O_4 when $n = 2, h = -2, S = 0.5, Ha = 10, \delta = 0.1, w = 0, \varepsilon = 0, P_r = 0.1, E_c = 0.01, \varphi = 5^\circ$

Approximates	q-HAM	LTCP-q-HAM	BVP4C
1 order	1.000847	1.001446	1.000786
2 order	1.001086	1.000058	1.000744
3 order	1.001167	1.000732	1.000744
4 order	1.001177	1.000686	1.000744
5 order	1.001178	1.000686	1.000744
6 order	1.001178	1.000686	1.000744

Table 6. Comparison of $-\bar{g}'(1)$ between q-HAM and LTCP-q-HAM for $n = 1.1, h = -0.9, S = 0.5, Ha = 50, \delta = 0.1, w = 0, \varepsilon = 0, \varphi = 5^\circ$.

		Au		Fe_3O_4		
P_r	E_c	q-HAM	LTCP-qHAM	q-HAM	LTCP-qHAM	BVP4C
0.5	1	1.52336273108	1.51350765323	1.52336273108	1.51350766836	1.51717817687
1	1	3.01023336320	3.01384328341	3.01023336320	3.01384331529	3.01461698607
2	1	5.87923137399	5.9384685834	5.87923137399	5.9384685710	5.95200370035
5	1	13.7276557447	14.3119436884	13.7276557447	14.3119436785	14.3334284523
1	0.5	1.50511668138	1.50692164676	1.50511668138	1.50692165158	1.50730849306
1	1.2	3.61228003537	3.61661197376	3.61228003537	3.61661197956	3.61754038329
1	2	6.02046672467	6.02768656316	6.02046672468	6.02768656124	6.02923397215
1	5	15.0511668138	15.0692164832	15.0511668138	15.0692165015	15.0730849303

Table 7. Comparison of $-\bar{g}'(1)$ between q-HAM and LTCP-q-HAM with Au for $n = 1.1, h = -1.26, S = 1, Ha = 100, \delta = 0.01, w = 0.01, \varepsilon = 0.001, \varphi = 12^\circ$

P_r	E_c	q-HAM	LTCP-q-HAM	BVP4C
0.5	1	1.52259102292	1.52204656620	1.52220372687
1	1	3.00816104964	3.01366523122	3.02068120677
2	1	5.87295921439	5.92585684374	5.94944357501
5	1	13.6842385762	14.2039739812	14.2388987838
1	0.5	1.50436754053	1.50682930355	1.51033642106
1	1.2	3.60951787027	3.61640146283	3.62482146152
1	2	6.01402851945	6.02735758201	6.04139584288
1	5	15.0179198304	15.0686163924	15.1037397441

Table 8. Comparison of $-\bar{g}'(1)$ between q-HAM and LTCP-q-HAM with Fe_3O_4 for $n = 1.1, h = -1.26, S = 1, Ha = 100, \delta = 0.01, w = 0.01, \varepsilon = 0.001, \varphi = 12^\circ$

P_r	E_c	q-HAM	LTCP-q-HAM	BVP4C
0.5	1	1.53631722722	1.52472320542	1.52941430817
1	1	3.03386424379	3.03399863250	3.03449706503

2	1	5.91780223471	5.94230315080	5.97477253772
5	1	13.7520776535	14.1458616836	14.2870599288
1	0.5	1.51723447977	1.51723788959	1.51724419543
1	1.2	3.64034698616	3.64087146653	3.64140063992
1	2	6.06531246732	6.0686064159	6.06902879604
1	5	15.1452175580	15.1482760616	15.1728313736

Table 9. The comparison of $-\bar{f}''(1)$ for $n = 3, h = -3, Ha = 10, P_r = 0.1,$ $E_c = 0.01, \delta = 0.1, w = 0.02, \varepsilon = 0.01, \varphi = 5^\circ$

S	q-HAM	LTCP-q-HAM	BVP4C
0	3.191698897084	4.721924867157	4.722056565409
0.5	4.870357728361	5.458861461486	5.171026835811
1.5	6.600915166112	6.221575690289	5.890627319671
2	7.218543891604	6.444418935022	6.180019541008
4	9.062755459888	6.938477789613	7.046600558228
6	10.33660050647	7.172804431174	7.646118574667

Table 10. The comparison of $-\bar{f}''(1)$ for $n = 3, h = -3, S = 1, P_r = 0.1,$ $E_c = 0.01, \delta = 0.1, w = 0.02, \varepsilon = 0.01, \varphi = 5^\circ$

Ha	q-HAM	LTCP-q-HAM	BVP4C
0	5.534567108213	5.769317166121	5.413985749409
100	5.774608879712	5.868140840938	5.596733959683
200	6.000795490982	5.957919509285	5.774191735604
300	6.214964554771	6.039840619352	5.946748896744
350	6.318015097697	6.078170049160	6.031299626409
550	6.706817272438	6.216368597740	6.358887984981
750	7.063688377435	6.334356433487	6.671101452309

Table 11. The comparison of $-\bar{f}''(1)$ for $n = 3, h = -3, Ha = 50, S = 1, P_r = 0.1,$ $E_c = 0.01, \delta = 0.1, \varepsilon = 0.01, \varphi = 5^\circ$

w	q-HAM	LTCP-q-HAM	BVP4C
0.02	5.656451759679	5.819942961723	5.506047396726
0.06	6.182353139054	6.062674455654	5.730750033108
0.08	6.374019472624	6.143500460889	5.816291998248
0.10	6.530378615155	6.190565259759	5.887118518898
0.15	6.800421388610	6.293706421903	6.010969183689

The impact of squeezing numbers on velocity and temperature profiles can be seen in Figures (2) and (3), there are two trends for the velocity profile in the interval $\tau \in [0,0.5]$: the flow velocity decreases as the squeezing number absolute value increases. In the other direction, the behavior of the second interval $\tau \in [0.5,1]$ is entirely different. It was observed that the velocity rises as the squeeze number grows, starting at a critical value $\tau_c \cong 0.5$. Conversely, the temperature profiles. It should be noted that when the squeeze number increases, there is a commensurate drop in temperature and boundary-layer thickness. This is due to S dependency on φ for the nanoparticles of Au and Fe_3O_4. It is evident from Figures (4) and (5) that there are two trends for $\bar{f}'(\tau)$. When the Hartmann number falls within the interval, $\tau \in [0,0.5]$, a decrease in flow velocity is observed. Conversely, in the interval, $\tau \in [0.5,1]$, the flow exhibits distinct behaviors, where an increase in the Hartmann number leads to a rise in velocity from a critical point $\tau_c \cong 0.5$. Additionally, the values of $\bar{g}(\tau)$ illustrate the influence of the Hartmann number and other studied parameters on temperature profiles. Notably, an increase in this parameter results in a temperature drop, consequently reducing the boundary layer thickness. As the inclination angle of the applied magnetic field increases, it leads to flattening velocity and temperature in the center of the channel, as shown in Figures (6) and (7). The temperature and flow velocity take low values compared to the results obtained for the vertical magnetic field. Figures (8) and (9) illustrate how the solid volume concentration of Au, and Fe_3O_4

nanoparticles affect the temperature distribution and flow velocity, respectively. It is discovered that the two figures of nanoparticle effect are identical, with high values of velocity occurring as solid volume concentration and temperature increase. Finally, the impact of $\varepsilon, \delta, E_c, P_r$ for various nanoparticle materials can be visualized.

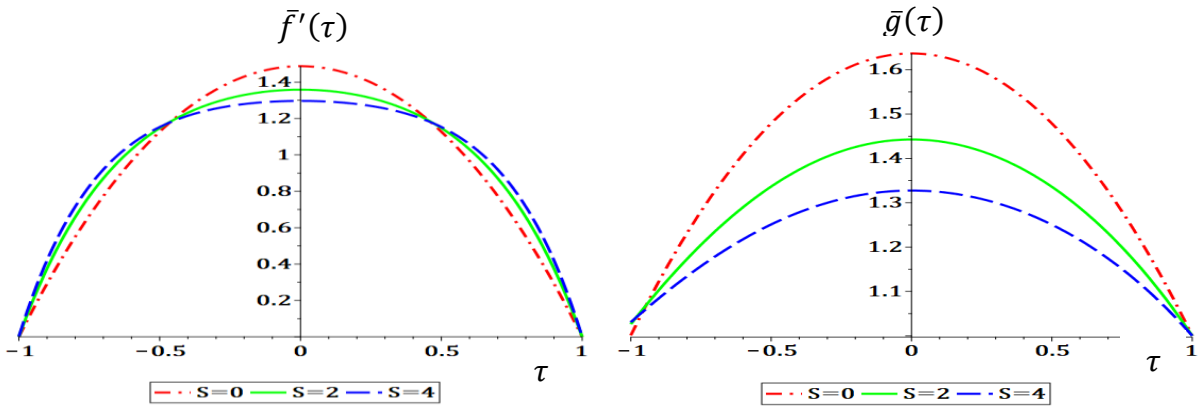

Fig. 2. $\bar{f}'(\tau)$ and $\bar{g}(\tau)$ for Fe_3O_4 $,\varphi = 45^{\circ}, E_c = 0.5, \varepsilon = 0.5, P_r = 7, Ha = 1, w = 0.05, \delta = 0.1$

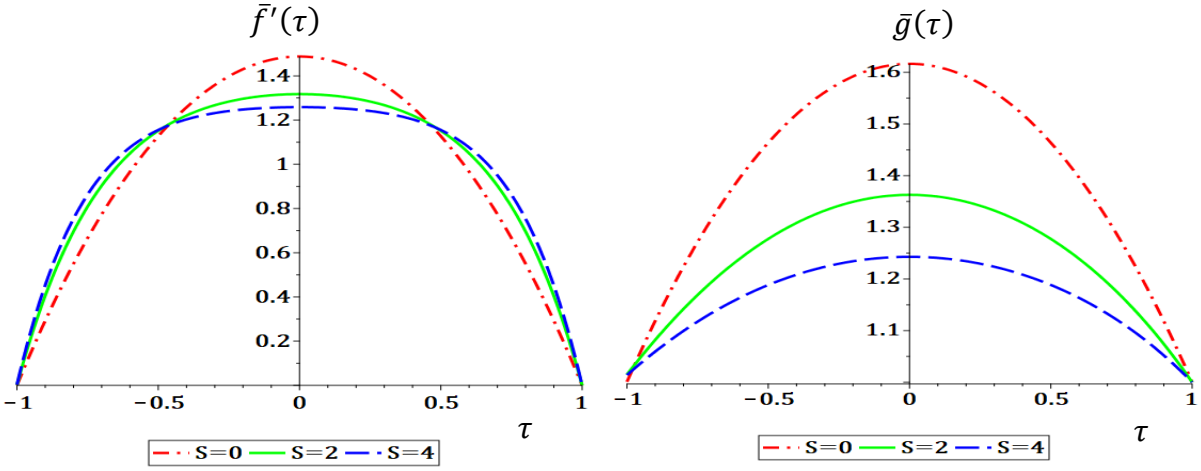

Fig. 3. $\bar{f}'(\tau)$ and $\bar{g}(\tau)$ for Au $,\varphi = 45^{\circ}, E_c = 0.5, \varepsilon = 0.5, P_r = 7, Ha = 1, w = 0.05, \delta = 0.1$

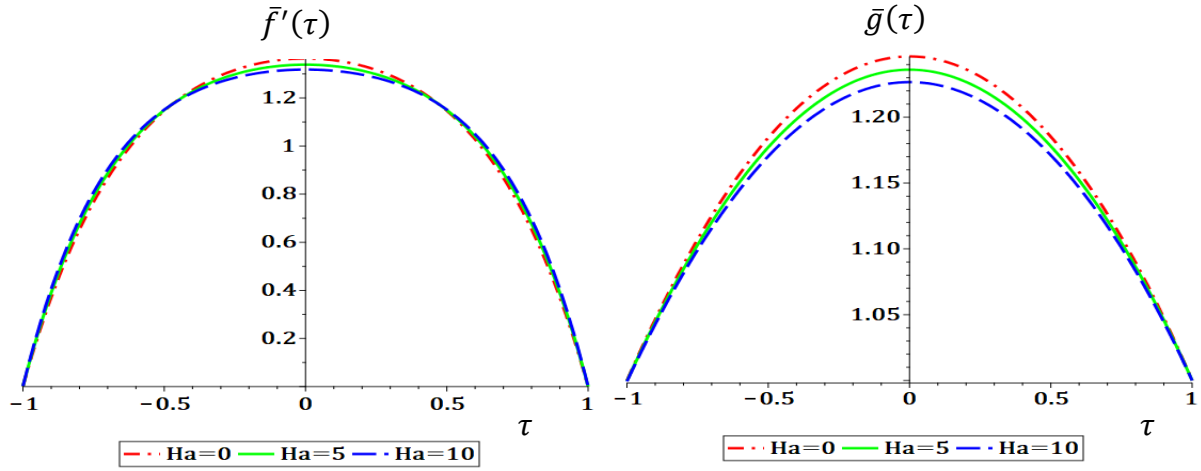

Fig. 4. $\bar{f}'(\tau)$ and $\bar{g}(\tau)$ for Fe_3O_4 $,\varphi = 45^{\circ}, E_c = 0.5, \varepsilon = 0.5, P_r = 7, S = 2, w = 0.05, \delta = 0.1$

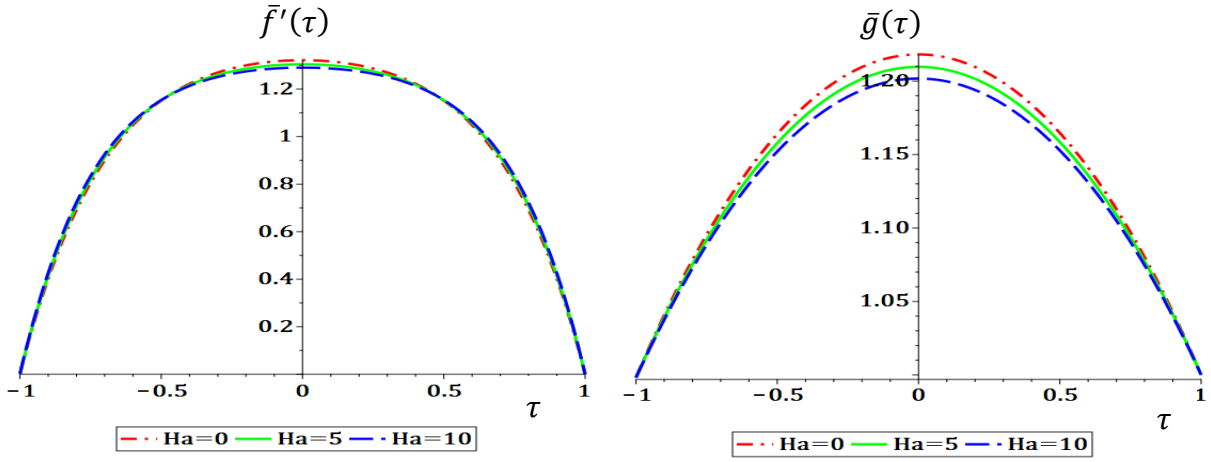

Fig. 5. $\bar{f}'(\tau)$ and $\bar{g}(\tau)$ for Au ,$\varphi = 45^{\circ}, E_c = 0.5, \varepsilon = 0.5, P_r = 7, S = 2, w = 0.05, \delta = 0.1$

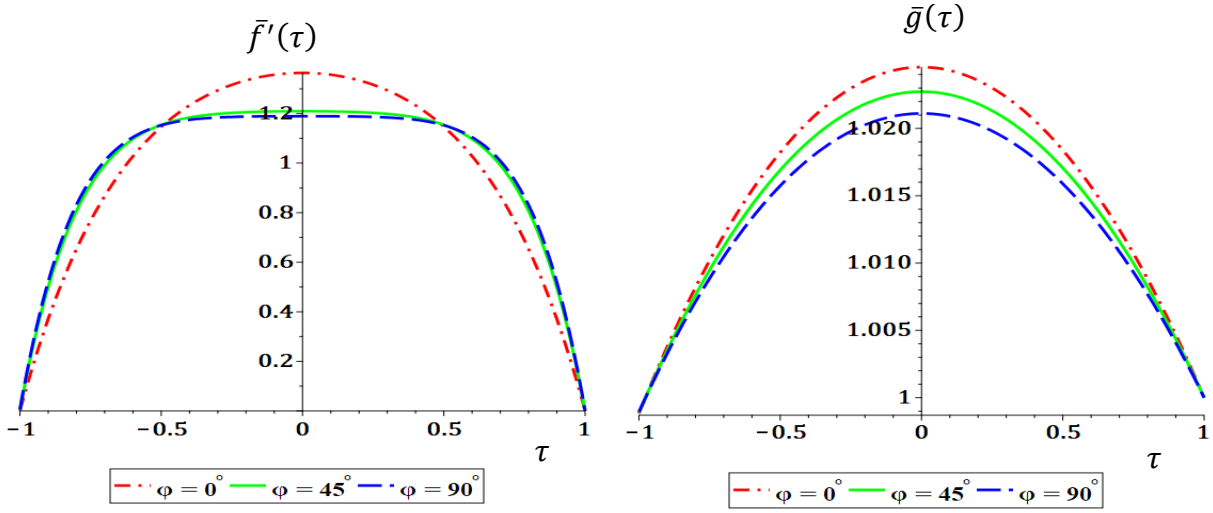

Fig. 6. $\bar{f}'(\tau)$ and $\bar{g}(\tau)$ for Fe_3O_4 ,$S = 2, E_c = 0.5, \varepsilon = 0.5, P_r = 7, Ha = 100, w = 0.05, \delta = 0.1$

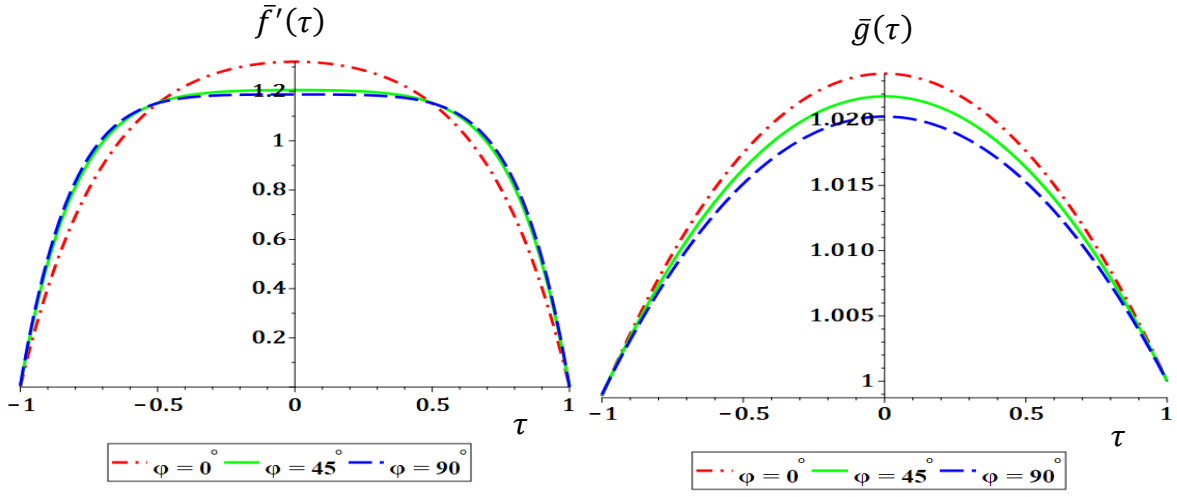

Fig. 7. $\bar{f}'(\tau)$ and $\bar{g}(\tau)$ for Au ,$S = 2, E_c = 0.5, \varepsilon = 0.5, P_r = 7, Ha = 100, w = 0.05, \delta = 0.1$

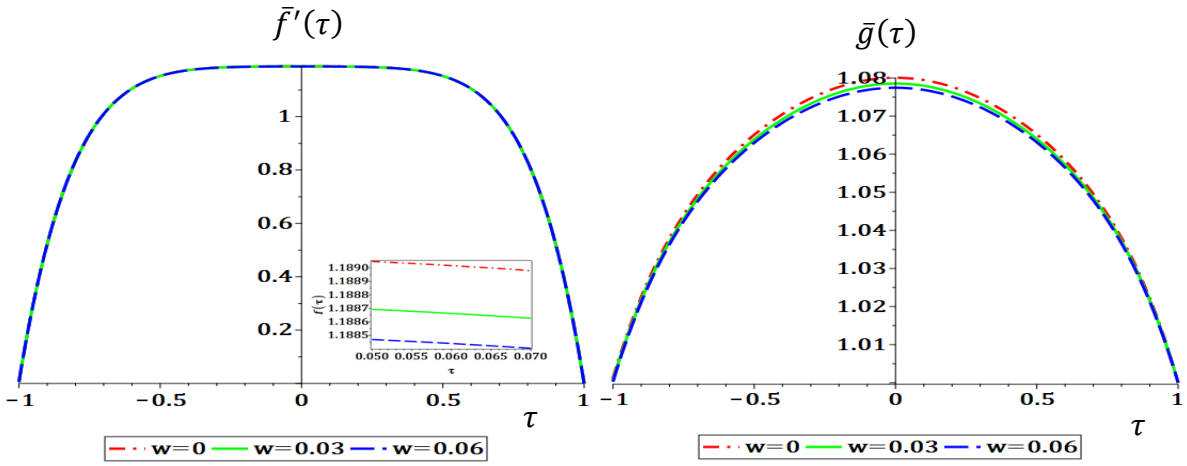

Fig. 8. $\bar{f}'(\tau)$ and $\bar{g}(\tau)$ for Fe_3O_4 ,$S = 3, E_c = 0.5, \varepsilon = 0.4, P_r = 7, Ha = 200, \varphi = 45^{\circ}, \delta = 0.1$

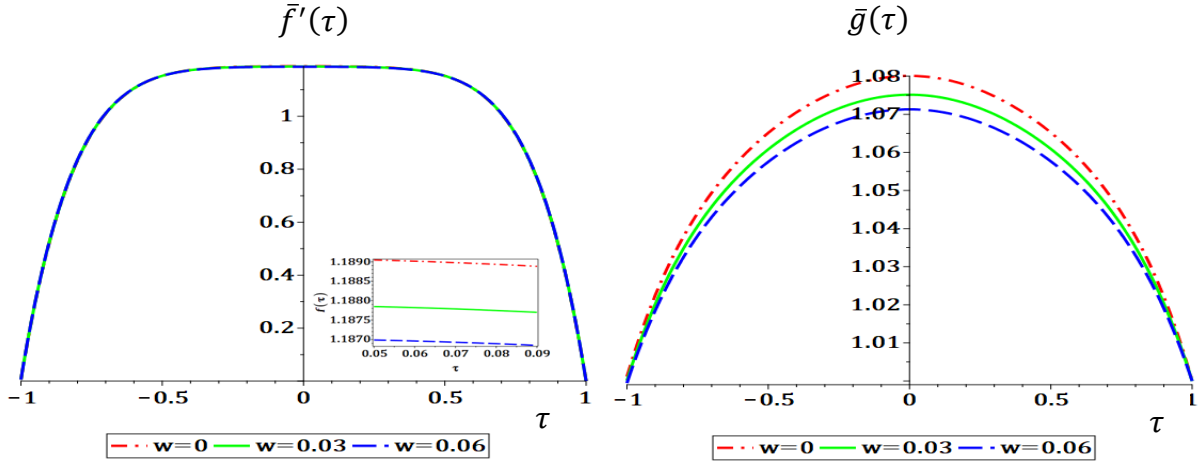

Fig. 9. $\bar{f}'(\tau)$ and $\bar{g}(\tau)$ for Au ,$S = 3, E_c = 0.5, \varepsilon = 0.4, P_r = 7, Ha = 200, \varphi = 45^{\circ}, \delta = 0.1$

The measure errors for q-HAM and LTCP-q-HAM can be indicated in **Table (12),** this Table demonstrates that the error measures of and for LTCP-q-HAM are accurate from q-HAM.

Table 12. The comparison of the errors of $\bar{f}(\tau)$ and $\bar{g}(\tau)$ between q-HAM, LTCP-q-HAM, when $n = 2, h = -1.9, Ha = 10, S = 0, \varphi = 1^{\circ}$, $w = 0.02, P_r = 0.1, E_c = 0.01, \delta = 0.1, \varepsilon = 0.01, \hat{\rho}_s = 19300$

	$\bar{f}(\tau)$		$\bar{g}(\tau)$	
Error	**q-HAM**	**LTCP-qHAM**	**q-HAM**	**LTCP-qHAM**
L_1	2.01×10^{-14}	9.57×10^{-17}	5.95×10^{-12}	8.84×10^{-14}
L_2	1.42×10^{-7}	9.79×10^{-9}	2.44×10^{-6}	2.97×10^{-7}
L_∞	2.11×10^{-7}	1.45×10^{-8}	3.17×10^{-6}	3.54×10^{-7}

7. Conclusions

In this work, the effects of inclined magnetic fields and variable thermal conductivity on heat transfer squeezing flow of unstable nanofluids have been investigated. The relevant nonlinear partial differential equations were transformed into a set of ordinary differential equations that have been solved analytically and numerically. The general conclusion can be submitted as follows:

- The nanoparticles Au and Fe_3O_4, when dispersed in the base fluid, H_2O, exhibit a similar influence on the obtained solutions. The presence of the base fluid significantly enhances the heat transfer properties, contributing to improved thermal performance.
- The incorporation of an inclined magnetic field, coupled with variable thermal conductivity, leads to a reduction in heat transfer efficiency.
- The convolution theory has a big impact on optimizing the results of solutions that solve the nanofluid problems.
- For certain values of the governing physical parameters, the solutions obtained using the proposed technique, are more accurate than those obtained using the q-homotopy analysis method.
- The comparison results of velocity and temperature profiles with the results of previous studies found that the results obtained from the proposed technique have a high level of agreement with the numerical solution.

References

[1] S. S. Reddy, K. Govardhan, G. Narender, and S. Misra, "Investigating the effect of a inclined magnetic field on heat and mass transmission in turbulent squeeze flow of UCM fluid between parallel plates," Arch. Thermodyn., pp. 169–178, 2024.DOI: https://doi 10.24425/ather.2024.152006.

[2] A. Dawar and H. Khan, "Analytical and numerical solutions of squeezing nanofluid flow between parallel plates: A comparison of IRPSM and HPM," Adv. Mech. Eng., vol. 16, no 12, 2024.DOI:https://doi.org/10.1177/16878132241304600.

[3] G. Domairry and M. Hatami, "Squeezing Cu–water nanofluid flow analysis betwee parallel plates by DTM-Padé Method," J. Mol. Liq., vol. 193, pp. 37–44, 201 DOI:http://dx.doi.org/10.1016/j.molliq.2013.12.034.

[4] A. Nouar, A. Dib, M. Kezzar, M. R. Sari, and M. R. Eid, "Numerical treatment of squeezin unsteady nanofluid flow using an optimized stochastic algorithm," Z. Naturforsch. A, vo 76, no. 10, pp. 933–946, 2021. DOI: https://doi.org/10.1515/zna-2021-0163

[5] S. Panda, L. A. AL-Essa, R. Baithalu, S. R. Mishra, and A. Saeed, "Velocity slip impact o the squeezing flow of water–CNTs and kerosene–CNTs nanofluids over a Riga surface," Taibah Univ. SCI, vol. 18, no. 1, 2024. DOI https://doi.org/10.1080/16583655.2024.2438324.

[6] A. Rehman, Z. Salleh, and M. Zeb, "Approximate analytical study of unsteady flow an heat transfer analysis of carbon nanotubes nanofluid over stretching sheet: Articl 3," Journal of Mathematical Sciences and Informatics, vol. 1, no. 1, pp. 25–38, 2021. DOI: http://dx.doi.org/10.46754/jmsi.2021.12.003.

[7] H. Shool, A. K. Raheem, and A. M. Al-Jaberi, "New Analytical and Numerical Solution for Squeezing Flow between Parallel Plates under Slip," Iraqi Journal of Science, 2024. DOI: http://dx.doi.org/10.24996/ijs.2024.65.3.34.

[8] N. Hedayati and A. Ramiar, "Investigation of two-phase unsteady nanofluid flow and hea transfer between moving parallel plates in the presence of the magnetic field usin GM," Challenges in Nano and Micro Scale Science and Technology, vol. 4, pp. 52–58 2016. DOI: http://dx.doi.org/10.7508/tpnms.2016.02.006.

[9] T. Hayat, T. Muhammad, A. Qayyum, A. Alsaedi, and M. Mustafa, "On squeezing flow o nanofluid in the presence of magnetic field effects," J. Mol. Liq., vol. 213, pp. 179–185 2016. DOI: http://dx.doi.org/10.1016/j.molliq.2015.11.003.

[10] A. G. Madaki, R. Roslan, M. S. Rusiman, and C. S. K. Raju, "Analytical and numerica solutions of squeezing unsteady Cu and TiO2-nanofluid flow in the presence of therma

radiation and heat generation/absorption," Alex. Eng. J., vol. 57, no. 2, pp. 1033–104(2018 DOI:.http://dx.doi.org/10.1016/j.aej.2017.02.011.

[11] M. Kezzar, I. Tabet, and N. Nafir, "Semi-analytical and numerical solutions for nonlinea problem of unsteady squeezing ferrofluid flow between stretchable/shrinkable walls unde external magnetic field and thermal radiation using differential transformatio method," Journal of Nanofluids, vol. 8, pp. 297–307, 2019. DOI http://dx.doi.doi:10.1166/jon.2019.1599.

[12] M. R. Eid, "Chemical reaction effect on MHD boundary-layer flow of two-phase nanoflui model over an exponentially stretching sheet with a heat generation," J. Mol. Liq., vol. 22(pp. 718–725, 2016. DOI: http://dx.doi.org/10.1016/j.molliq.2016.05.005

[13] M. R. Eid and K. L. Mahny, "Unsteady MHD heat and mass transfer of a non-Newtonia nanofluid flow of a two-phase model over a permeable stretching wall with hea generation/absorption," Adv. Powder Technol., vol. 28, no. 11, pp. 3063–3073, 2017. DOI: https://doi.org/10.1016/j.apt.2017.09.021.

[14] K. Al-Farhany, M. F. Al-Dawody, D. A. Hamzah, and N. H. Hamza, "Numerical study o nanofluid natural convection in a partially heated tall enclosure," IOP Conf. Ser. Mater. Sc Eng., vol. 928, no. 2, p. 022137, 2020. DOI: https://doi:10.1088/1757-899X/928/2/022137

[15] Y. S. Daniel, Z. A. Aziz, Z. Ismail, and F. Salah, "Thermal radiation on unsteady electrica MHD flow of nanofluid over stretching sheet with chemical reaction," J. King Saud Univ Sci., vol. 31, no. 4, pp. 804–812, 2019. DOI: https://doi.org/10.1016/j.jksus.2017.10.002

[16] S. Hussain, A. Shah, A. Ullah, and F. Haq, "The q-homotopy analysis method for a solutio of the Cahn–Hilliard equation in the presence of advection and reaction terms," J. Taiba Univ. SCI, vol. 16, no. 1, pp. 813–819, 2022 DOI:https://doi.org/10.1080/16583655.2022.2119746.

[17] B. Wu and Y. Qian, "Padé Approximation Based on Orthogonal Polynomial, in Proceedings of 2016 International Conference on Modeling, Simulation an Optimization Technologies and Applications (MSOTA2016), 2016. DOI https://doi.org/10.2991/msota-16.2016.54.

[18] H. A. A. Namoos and A. M. Jasim, "The analytical improvement of q-homotopy analysi method for magneto-hydrodynamic (MHD) Jeffrey Hamel nanofluid flow," Adv. Res Fluid Mech. Therm. Sci., vol. 119, no. 2, pp. 32–55, 2024. DOI https://doi.org/10.37934/arfmts.119.2.3255.

[19] A. Jasim and A.-S. J. A.-S. Majeed, "New analytical solution formula for heat transfer o unsteady two-dimensional squeezing flow of a Casson fluid between parallel circula plates," Journal of Advanced Research in Fluid Mechanics and Thermal Sciences, vol. 64 no. 2, pp. 219–243, 2019. Available https://semarakilmu.com.my/journals/index.php/fluid_mechanics_thermal_sciences/articl e/view/3650

Journal of Basrah Researches (Sciences) **51**(1), 68 (2025)
DOI: https://doi.org/10.56714/bjrs.51.1.6

تأثيرنظرية الألتواء في انتقال الحرارة لتدفق الموائع النانوية غير المستقرة مع وجود مجال مغناطيسي مائل

حيدر عبد الرزاق ناموس*، عبير مجيد جاسم.

قسم الرياضيات، كلية العلوم ، جامعة البصرة، البصرة، العراق.

معلومات البحث

الاستلام 5 كانون الثاني 2025
المراجعة 7 شباط 2025
القبول 15 شباط 2025
النشر 30 حزيران 2025

الكلمات المفتاحية

طريقة التحليل كيوهوموتوبي، تحويل لابلاس ، نظرية الألتواء، تقريب بادي، التوصيل الحراري المتغير، الانضغاط غير المستقر،زاوية ميل المجال المغناطيسي المطبق.

الملخص

تبحث الدراسة في انتقال حرارة الموائع النانوية غير المستقرة في تدفق مضغوط بين لوحين متوازيين بأستخدام الماء كسائل أساسي مع جزيئات الذهب (Au) والمغنتيت (Fe_3O_4) النانوية. تم استخدام منهج تحليلي جديد (LCP-q-HAM) يجمع بين طريقة تحليل (q-HAM) وتحويل لابلاس ونظرية الألتواء وتقريب بادي لحل المعادلات التفاضلية غير الخطية التي تتضمن التوصيل الحراري وتأثيرات المجال المغناطيسي. تتم مقارنة الحلول التحليلية والعددية بأستخدام BVP4C من خلال الجداول والرسوم البيانية وتحليل توزيعات درجة الحرارة والسرعة لمعلمات مختلفة مثل جزء حجم الجسيمات النانوية ورقم هارتمان ورقم الضغط وزاوية المجال المغناطيسي والموصلية. وتؤكد النتائج فعالية الطريقة التحليلية.

Citation: H. A. A. Namoos , A. M. Jasim, J. Basrah Res. (Sci.) **51**(1), 68 (2025).
DOI:https://doi.org/10.56714/bjrs.51.1.6

***Corresponding author email :** haedirnamoos@gmail.com

N: 1817-2695 (Print); 2411-524X (Online)
ine at: https://jou.jobrs.edu.iq